PREDICTION OF MOISTURE CONTENT IN CORN LEAVES BASED ON HYPERSPECTRAL IMAGING AND CHEMOMETRIC ANALYSIS

Y. Sun, S. S. Chen, J. F. Ning, W. T. Han, P. R. Weckler

ABSTRACT. *The moisture content of corn leaves under different moisture treatments was predicted with a hyperspectral imaging technique. The reflectance spectra of corn leaves were acquired in the spectral range of 900 to 1700 nm with a hyperspectral imaging system, and the moisture content of the same samples was acquired with the traditional oven-drying method. Partial least square regression (PLSR), multiple linear regression (MLR), and back-propagation artificial neural network (BP-ANN) models were used to analyze the correlation between spectral data and moisture content. Correlations were found between moisture content of the corn leaves and hyperspectral information; the coefficient of determination was greater than 0.85, with RMSEC and RMSEP values less than 0.01. This work provides an effective method for prediction of moisture content of corn leaves using a hyperspectral imaging technique.*

Keywords. *Chemometric analysis, Corn leaves, Hyperspectral imaging, Moisture content.*

Water is one of the most important factors for crop growth, and its measurement is an indicator of crop status. Obtaining quantitative moisture content information on crop growth can also indicate the soil's moisture condition. This can have a positive role in guiding crop irrigation and has potential significance for water management and early drought warning in agriculture, horticulture, and forestry (Peñuelas et al., 1993, 1996). Soil water deficits lead to reductions in soil productivity, while crop water stress leads to declines in crop yield and quality. Therefore, a rapid, accurate, and quantitative method to assess crop water status will contribute to improved crop irrigation management.

Corn is one of the world's major crops. It is not only an important food source but also a feedstock for bio-energy production. Reliable corn yield and quality is of great practical significance for world food and energy security. Corn production has a high demand for water; however, in China, two-thirds of corn production is located in the arid and semi-arid areas of the country. This means that the water intake of corn is not effectively guaranteed, resulting in loss of corn yield and quality. Detection of corn moisture status helps with water supply management in the growth of corn.

Submitted for review in February 2014 as manuscript number ITSC 10645; approved for publication by the Information, Technology, Sensors, & Control Systems Community of ASABE in May 2015.

The authors are **Yu Sun,** Graduate Student, College of Mechanical and Electronic Engineering, **Shanshan Chen,** Graduate Student, and **Jifeng Ning,** Associate Professor, College of Information Engineering, and **Wenting Han,** Professor, College of Mechanical and Electronic Engineering and Institute of Soil and Water Conservation, Northwest A&F University, Yangling China; **Paul R. Weckler, ASABE Member,** Associate Professor, Department of Biosystems and Agricultural Engineering, Oklahoma State University, Stillwater, Oklahoma. **Corresponding author:** Wenting Han, Northwest A&F University, 26 Xinong Road, Yangling, China; phone: 86-29-87091325; e-mail: hanwt2000@126.com.

The traditional methods of determining moisture content include oven-drying, distilling, and so on（Li et al., 2010). However, these methods are time-consuming and unsuitable for use in field production. When crops are experiencing a significant water shortage, it is usually too late to irrigate. Therefore, it is useful to develop a rapid testing method to detect crop water status.

Researchers have investigated different spectral bands for water sensitivity (Carter, 1991; Danson et al., 1992; Jackson, 1984; Hatfield and Pinter, 1993). The spectral bands at 950-970 nm, 1150-1260 nm, 1450 nm, 1950 nm, and 2250 nm have shown promise in estimating water content in certain species. Hyperspectral imaging technology is a combination and expansion of digital image sensing and spectroscopy methods (Gowen et al., 2007; Kim et al., 2011; Cheng et al., 2004, Xie et al., 2013). In each band of the spectrum, the hyperspectral imaging technique obtains a three-dimensional gray-scale image that contains a two-dimensional image and third-dimensional hyperspectral data. Compared to single-spectrum technology or digital image processing, hyperspectral imaging provides spatial and spectral information on the samples, including color, shape, texture, and internal information (Geladi et al., 2004; Noh and Lu, 2007; Liu and Ngadi, 2013). Studies have shown that hyperspectral imaging can be used to detect target moisture content (Qiao et al., 2007; Zhang et al., 2011). Multivariate calibration methods are used to analyze the correlation between hyperspectral data and moisture content. The main modeling methods include partial least square regression (PLSR), multiple linear regression (MLR), and back-propagation artificial neural network (BP-ANN). This research compared the three modeling methods to find the optimal multivariate calibration model. The overall objectives of this research were to:

- Acquire hyperspectral images of corn leaves.
- Assess the accuracy of reflectance information in estimating plant water content in corn leaves.

Vol. 58(3): 531-537 ISSN 2151-0032 DOI 10.13031/trans.58.10645

- Develop and validate models for moisture content prediction.

MATERIALS AND METHODS

MATERIALS

The test site was located in China at the Research Institute of Arid Region in Agriculture, Northwest A&F University, (108° 4′ E, 34° 17′ N). The test date was August 16, 2013. The variety of planted corn was Xianke 858 summer corn. Corn plants were grown in a greenhouse in standard flats. The ninth leaf positions of corn plants at large bell growth were selected as samples that can better represent the water status of the plant (Wang and Bai, 2005; Tian et al., 2005). Samples of 115 corn leaves were selected from 115 corn plants. The leaf was cut from the base and placed in a storage bag in a sealed box with ice to maintain the moisture content. Wet weight (W_f) was recorded using an electronic scale (PTX-JA-110, Fuzhou Huazhi (Polestar Balance) Electronic Scale Co., Fuzhou, China) with an accuracy of 0.001 g. Hyperspectral images of the leaves were collected afterward.

MOISTURE CONTENT MEASUREMENT

Moisture content was determined using the oven-drying method. After the collection of hyperspectral images, the corn leaves were bagged in paper and placed in a drying oven at 105°C for half an hour. They were then kept at a constant temperature of 85°C to continue drying and weighed at scheduled intervals until no change in weight was observed. Weight change was assumed to be due to loss of water content. Gravimetric moisture content (GMC) was computed using the following equation:

$$\text{MC}\ (\%) = [(W_f - W_d)/W_f] \times 100 \quad (1)$$

where W_f is wet weight (g), and W_d is dry weight (g).

HYPERSPECTRAL REFLECTION IMAGING SYSTEM

A line-scan hyperspectral reflection imaging system, shown in figure 1, was used to acquire hyperspectral reflection images of corn leaves. The imaging system consisted of a hyperspectral imaging unit, a light source, a sample handling platform, and a computer control system. The hyperspectral imaging unit contained a back-illuminated CCD (charge-coupled device) camera (320 × 256 pixel resolution, XEVA2616, Xenics, Leuven, Belgium) and an imaging spectrometer (ImSpector N17E, Spectral Imaging, Ltd., Oulu, Finland). The CCD detector covered an effective spectral range of 900 to 1700 nm with 2.8 nm spectral resolution and a 30 μm slit width coupled with a zoom lens. The light source was composed of a 150 W DC, 3250K halogen lamp. The sample handling platform consisted of a horizontal motorized stage with flat black cardboard (2 mm thick) fixed on the stage. The computer was used to control the sample handling platform and acquire images. The entire system was operated in a chamber, the walls of which were painted black to avoid unwanted reflections and ambient light interference during image capture.

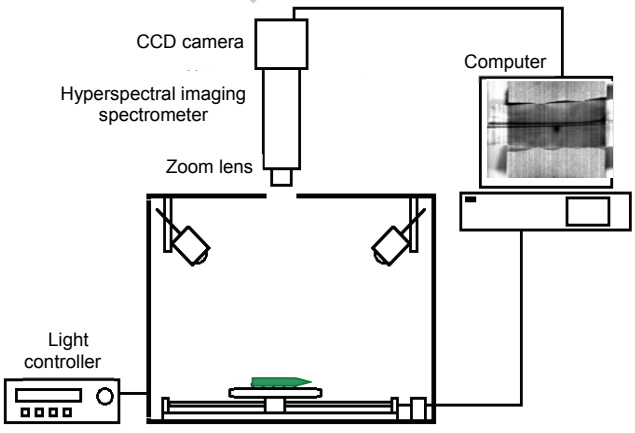

Figure 1. Schematic diagram of hyperspectral imaging system.

SAMPLING OF HYPERSPECTRAL IMAGES

Hyperspectral images were sampled using Spectral SECN-V17E software (Gilden Photonics, Ltd., Glasgow, U.K.). To collect clear spectral images with no distortion, the zoom lens, the speed of the platform, the exposure time, and the light source were adjusted to provide optimum image quality. The exposure time was adjusted to 10 ms, and the speed of the platform was adjusted to 20 mm s^{-1} throughout the test.

During hyperspectral image acquisition, the leaf samples were placed on the sampling handling platform. The hyperspectral image was captured line by line as the platform continuously moved the sample through the view of field of the camera to determine the size of the vertical axis (y) of the spatial dimension, while the horizontal axis (x) of the spatial dimension of the image was fixed. The scanned hyperspectral data had a real spectral range between 865 and 1712 nm with about 3.3 nm spectral resolution, which is slightly greater than the nominal value for the CCD detector. Each hyperspectral image was stored as a three-dimensional image (x, y, γ). The spatial component (x, y) included 320 × 256 pixels, and the spectral component (γ) included 256 bands.

All the hyperspectral images were calibrated with white and dark references. The dark reference was used to remove the dark current sensitive effect of the CCD detector. The corrected image (R) was calculated using the following equation:

$$R = \frac{R_o - R_b}{R_w - R_b} \quad (2)$$

where R_o is the original acquired hyperspectral image, R_w is the white reference image obtained with a Teflon white board with 99% spectral reflection, and R_b is the dark image obtained by turning off the light source and covering the lens with a black lens cap (Baiano et al., 2012; Karimi et al., 2012).

HYPERSPECTRAL IMAGING PROCESS

The hyperspectral image data were processed with ENVI 4.7 (Environmental Research Systems Institute, Inc., Redlands, Cal.). In the hyperspectral images, the leaf and

background had different spectral characteristics. A masking method was used to extract the leaf area as the region of interest (ROI) and eliminate the effects of background (Lorente et al., 2013). In this method, a binary mask was created using a band ratio method. The band ratio method achieves a relative wavelength image by obtaining the ratio of a wavelength image with another wavelength image. The image bands selected for the band ratio were 1051 nm (peak value) and 1446 nm (valley value), as shown in spectral data plots. The mask was acquired with a set threshold 1.5 based on the band ratio image. In the mask, the background area is 0, while the leaf area is 1 and applied to extract the ROI. The size of the ROI was about 15 cm × 6 cm in order to collect efficient spectral data and remove the leaf edge effects. The average spectra can be calculated from the ROI. In this work, 221 bands (from 915 to 1680 nm) were selected for removing the high level of noise and reducing data redundancy in this range (Hernández-Hierro et al., 2013; Gamal and Jens, 2008).

DATA ANALYSIS

DATA PREPROCESSING

A variety of noise sources degraded the data signal during the hyperspectral image acquisition process. Therefore, it was necessary to preprocess the raw spectral data using the appropriate mathematical methods to improve the signal to noise ratio. In this study, seven data preprocesses including Savitzky-Golay smoothing (SG), standard normal variant (SNV), multiplicative scatter correction (MSC), detrending, baseline, first-derivative filtering (1-Der), and second-derivative filtering (2-Der), which are widely used in spectral preprocessing, were tested to eliminate noise from the raw spectra of 115 corn samples with Unscrambler 10.2 (Camo Software, Oslo, Norway).

The performance of the prediction models was evaluated using evaluation indicators, including the coefficients (R_c and R_p) and root mean square errors (RMSEC and RMSEP) of the calibration set and the validation set, respectively, and the number of latent variables required. The number of latent variables required was determined by using the minimum value of the predicted residual error sum of squares (Keshava, 2003; Liang et al., 2012). Coefficient R_p and the RMSEP of the validation set were calculated using the following equations:

$$R_p = \sqrt{1 - \frac{\sum_{i=1}^{N} (Y_{Ti} - Y_{Pi})}{\sum_{i=1}^{N} (Y_{Ti} - Y_m)}} \quad (3)$$

$$\text{RMSEP} = \sqrt{\frac{1}{N} \sum_{i=1}^{N} (Y_{Ti} - Y_{Pi})^2} \quad (4)$$

where Y_{Pi} is the predicted value of the samples, Y_{Ti} is the value of the reference data, Y_m is the average value of the reference data, and N is the number of samples.

SUCCESSIVE PROJECTIONS ALGORITHM

The successive projections algorithm (SPA) is a forward variable selection algorithm used to solve collinearity problems. This algorithm applies a vector projection operation in a specific vector space to select subsets of variables with minimum collinearity. The SPA consists of two phases. The first phase generates subsets of variables by conducting projections on the instrumental response data. The basic principle of variable selection for SPA is selecting the new variable that has the maximum projection value on the orthogonal subspace of the previous selected variables among all the remaining variables. The second phase is an evaluation of the candidate subsets of variables obtained in the first phase. The best subset of variables can be determined by multiple linear regression (MLR) calibration based on the smallest root mean squared error of cross-validation in the calibration set. The details of SPA can be found in the literature (Araújo et al., 2001; Galvão et al., 2007). The Statistics Toolbox of Matlab 7.1 (The Mathworks Inc., Natick, Mass.) was used.

PARTIAL LEAST SQUARES REGRESSION

Partial least square regression (PLSR) is useful for predicting a set of dependent variables from a large set of independent variables. The PLSR method performs particularly well when the various X variables express common information, or when there is a large amount of correlation or even collinearity (Nicolai et al., 2007; Talens et al., 2013). In this study, the values of moisture content of the dataset (Y) were used as the dependent variables, and full-band spectra and sensitive wavelengths selected by SPA of the dataset (X) were used as the independent variables. Unscrambler 10.2 (Camo Software, Oslo, Norway) was used to develop the PLSR model.

MULTIPLE LINEAR REGRESSION

Multiple linear regression (MLR) develops a correlation analysis between two or more independent variables and a dependent variable. The performance of MLR depends largely on the input of the regression model. Optimal wavelength selection can improve the advantage of MLR (Wang et al., 2007). The Statistics Toolbox of Matlab 7.1 (The Mathworks Inc., Natick, Mass.) was used.

BACK-PROPAGATION ARTIFICIAL NEURAL NETWORK

The back-propagation artificial neural network (BP-ANN) is the most common version of artificial neural network (ANN). Each neuron is a processing unit that transforms input into output data by an activation function. A typical BP-ANN generally consists of an input layer, one or more hidden intermediate layers, and an output layer. In this method, the signal is fed forward, and the error is propagated backward. The use of BP-ANN for variable selection is a causal index analysis of the trained ANN model to obtain a quasi-quantitative estimate of the direction and magnitude of the influence of each ANN input on each ANN output. The Neural Network Toolbox of Matlab was used to build the BP-ANN model.

Table 1. Statistical analysis of moisture content of samples.

Sample Set	No. of Observations	Min. (%)	Max. (%)	Mean (%)	SD
Total	113	68.95	78.70	74.22	0.0215
Modeling	82	70.11	78.70	74.17	0.0223
Prediction	31	68.95	77.72	74.33	0.0221

Results and Discussion

Hyperspectral Imaging

Two anomalous samples were excluded from the 115 sample leaves using Unscrambler 10.2 (Camo Software, Oslo, Norway). The range, mean, and standard deviation of the moisture content of the target corn leaves are shown in table 1. Figure 2 shows the average reflectance spectra in the range of 915 to 1680 nm for the 113 leaves processed. In general, all recorded spectra had the same shape and showed a characteristic sensitive wavelength at around 1450 nm, which is the multiple frequency absorption peak of water's O-H. However, we cannot determine leaf moisture just from the spectral reflectance. The spectral curves all show a similar pattern, and small differences in reflectance magnitude can be observed among the spectral profiles of the samples.

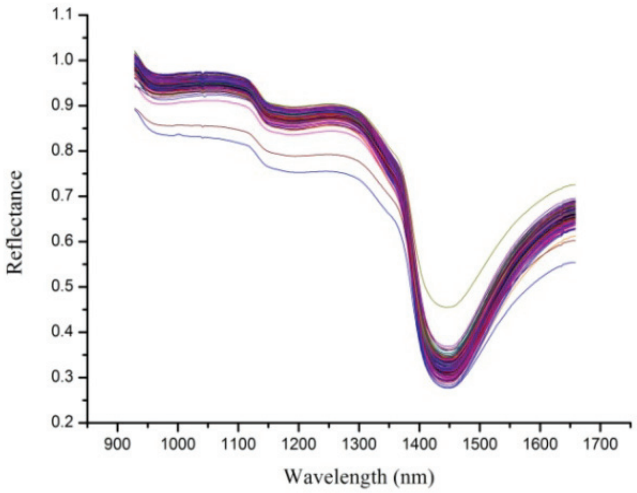

Figure 2. Spectral reflectance of corn leaves (n = 113).

Hyperspectral Image Spectral Pretreatment

In this study, seven pretreatment methods were applied to the spectral data, and individual calibration models were built afterward using PLSR. The results are presented in figures 3, 4, and 5. The performance of the calibration set and validation set based on the raw spectra were in better accord when the correlation coefficients were greater than 0.86 and the RMSE values were less than 0.11. However, the seven preprocessing treatments tested did not enhance the calibration model. Comparison between the raw hyperspectral data and the seven pretreatment methods showed that the multivariate calibration model based on the raw full-band hyperspectral data achieved the best performance.

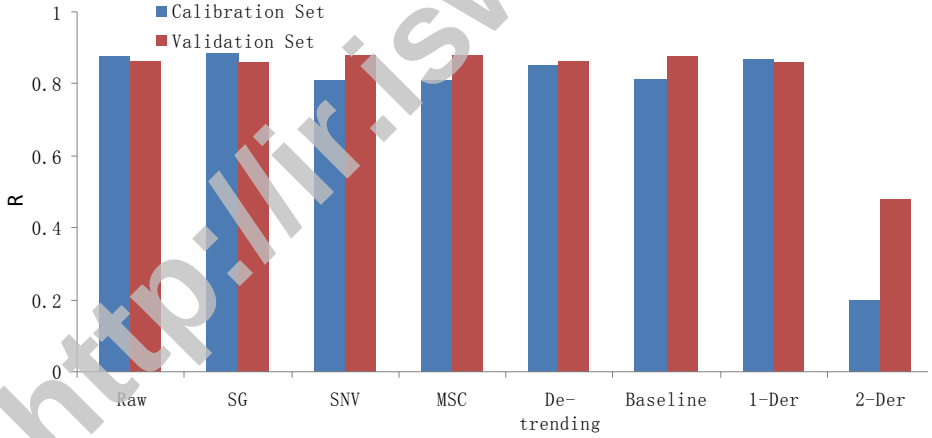

Figure 3. Comparison of R for eight PLSR models after preprocessing.

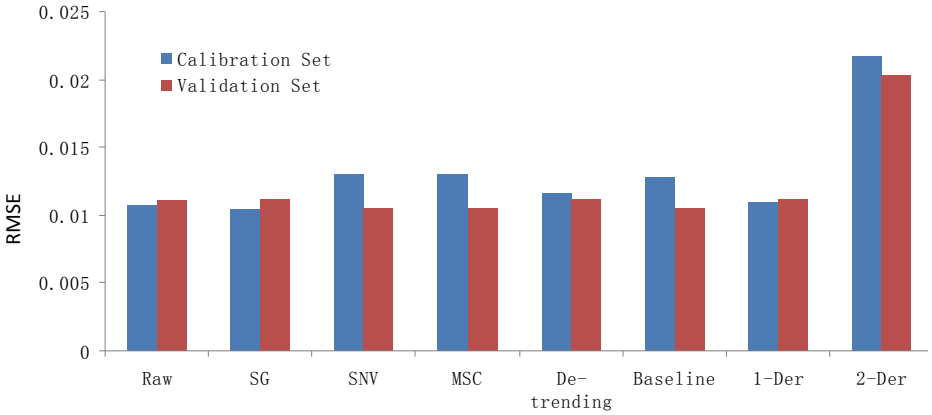

Figure 4. Comparison of RMSE for eight PLSR models after preprocessing.

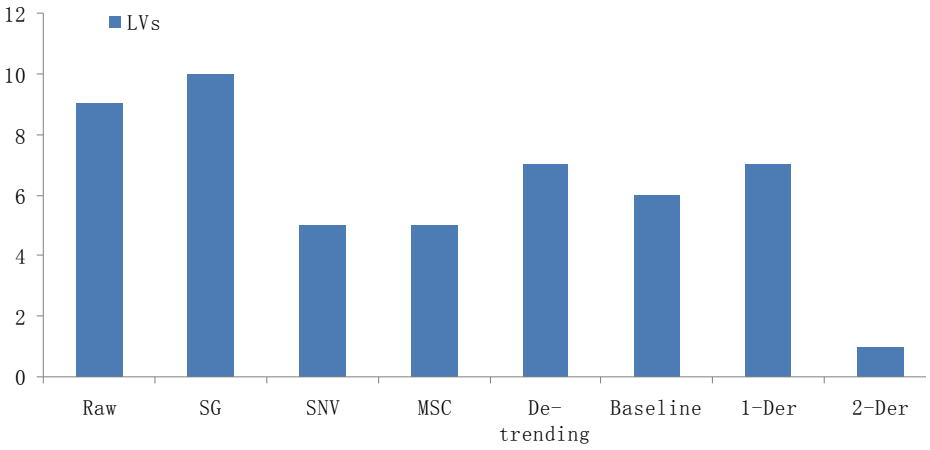

Figure 5. Number of latent variables (LVs) for eight PLSR models after preprocessing.

These results showed that the established PLSR model based on raw hyperspectral image data can apply to cross-validation and prediction models. This also reflects the overall trend of the data between spectra and moisture content.

The spectral data preprocessed with second-derivative filtering presented the worst result; the correlation coefficients of the calibration set and validation set were both less than 0.5. Therefore, second-derivative preprocessing is not a good fit for the hyperspectral image data model. The correlation coefficients of the calibration set and validation set for the other pretreatments were all greater than 0.8, which demonstrates that the model has the ability to detect corn moisture content using hyperspectral imaging.

Sensitive Wavelength Selection by SPA

The successive projections algorithm (SPA) was applied to the optimal band selection to reduce the spectral data dimensionality while finding the most important information contained in the lower-dimensional data space that would be most influential on the moisture measurement of corn leaves. The numbers of wavelengths selected for the moisture content prediction of corn leaves by the SPA are plotted in figure 6. When seven wavelengths (1466, 1330, 1088, 1589, 1413, 935, and 961 nm, sorted according to contribution to the model) were included in the spectral selection, the RMSE was less than 0.014. The seven sensitive wavelengths spanned nearly the entire spectral range of the sensor (900-1700 nm). The selected sensitive wavelengths are plotted in figure 7.

Partial least squares regression (PLSR), multi-linear regression (MLR), and back-propagation artificial neural network (BP-ANN) were used to build calibration models for predicting the moisture content of corn leaves using the sensitive wavelengths selected by the SPA.

Prediction of Moisture Content

The Neural Network Toolbox of Matlab was used to build the MLR model and the BP-ANN model. In the BP-ANN model, the number of hidden layer nodes was set to four in the training mode, and the output layer node corresponded to moisture content; therefore, the final neural

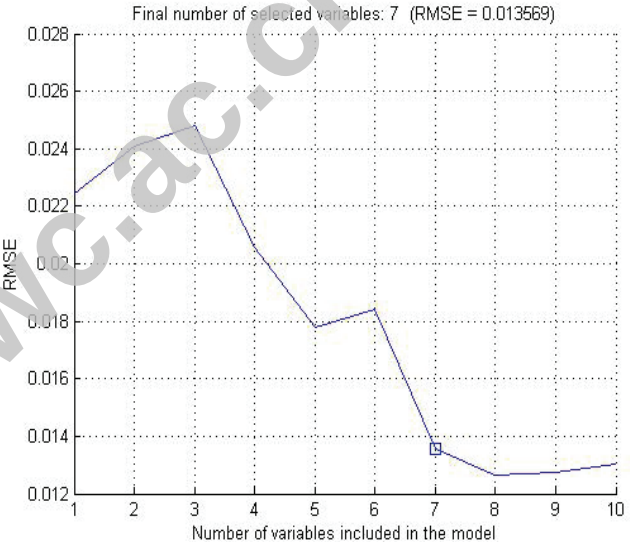

Figure 6. Selected number of wavelengths.

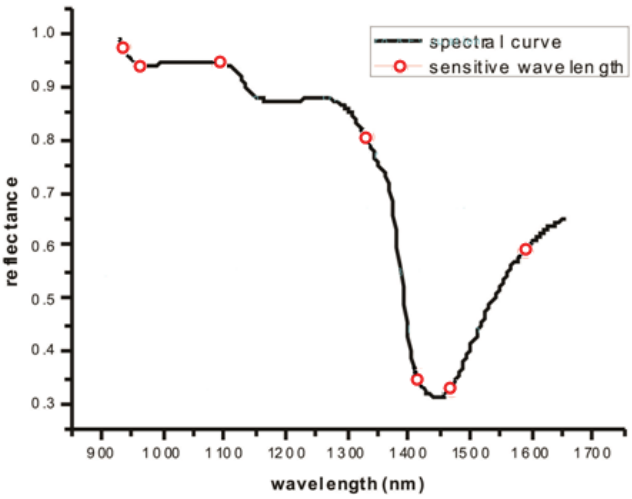

Figure 7. Selected sensitive wavelengths.

network structure was 7-4-1. The learning rate was set to 0.6, the number of iterations was 1000, and the deviation of the target was 10-5. Figures 8 and 9 summarize the results of the PLSR, MLR, and BP-ANN models using the seven sensitive wavelengths selected by the SPA. Comparing the PLSR model using the seven sensitive wavelengths to the PLSR model using the full spectra, the R_p of the calibration set and the validation set both decreased to less than 0.05; however, the number of latent variables decreased from 9 to 6, and the number of wavelengths was reduced by 96.8%.

The SPA-MLR and SPA-BP-ANN models had similar RMSEP values (RMSEP = 0.01083 for SPA-MLR and 0.01076 for SPA-BP-ANN) and correlation coefficients (R_p = 0.8705 for SPA-MLR and 0.8784 for SPA-BP-ANN) for the validation set. The RMSEP (0.01139) for the PLSR model using the full spectra was higher than that for the SPA-MLR and SPA-BP-ANN models. As measured by R_p and RMSEP, the SPA-BP-ANN model with the seven sensitive wavelengths had the best result for moisture content (R_p = 0.8784, RMSEP = 0.01076); however, the RMSEC (0.01170) of the calibration set was greater than that of SPA-MLR. Compared to the SPA-PLSR and SPA-MLR models, the SPA-BP-ANN model had a lower RMSEP. Figures 10 and 11 show the validation and calibration results for the BP-ANN model based on the seven sensitive wavelengths selected by the SPA.

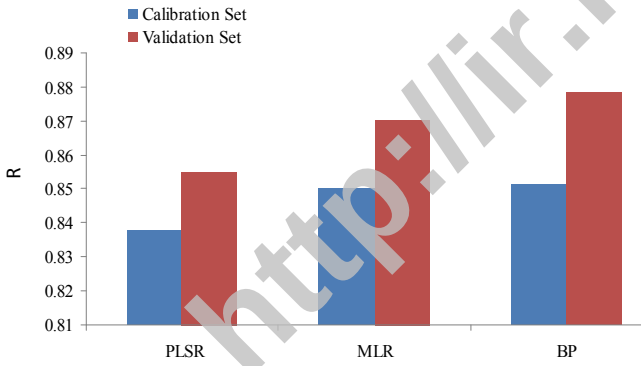

Figure 8. Comparison of R for three models based on SPA.

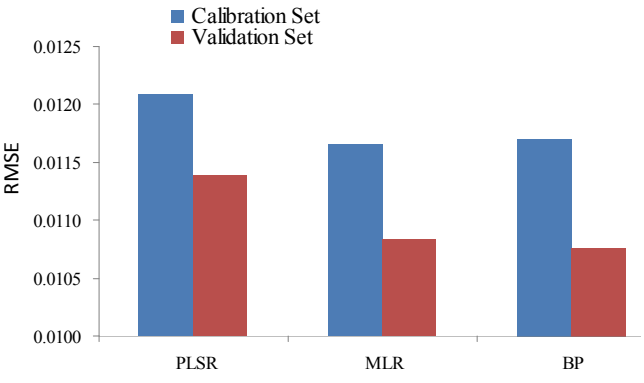

Figure 9. Comparison of RMSE for three models based on SPA.

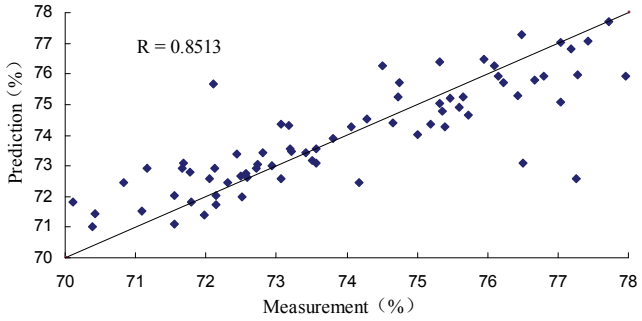

Figure 10. Measured vs. SPA-BP-ANN values for calibration.

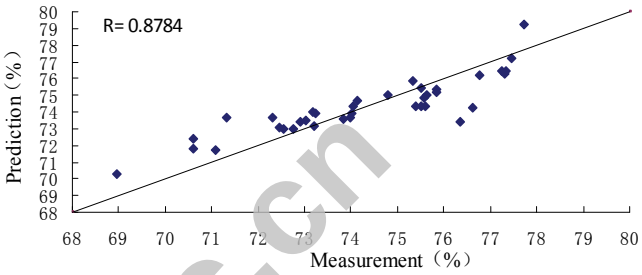

Figure 11. Measured vs. SPA-BP-ANN values for validation.

CONCLUSION

In this article, hyperspectral imaging technology in combination with chemometric methods was used to determine the moisture content of corn leaves. After hyperspectral image acquisition, the average spectra obtained from the ROI of corn leaves was used for data processing. Seven different preprocessing methods were tested to modify the spectral data prior to building the corresponding PLSR models. The results showed that the prediction performance of the PLSR models was optimal when based on the raw spectral data compared to the seven preprocessing methods, which means that other preprocessing methods cannot help to improve the performance of the PLSR model in this work. The SPA method was used to select seven sensitive wavelengths (1466, 1330, 1088, 1589, 1413, 935, and 961 nm) out of the raw hyperspectral data. The PLSR, MLR, and BP-ANN models were built based on the sensitive wavelengths selected. Validation results showed that the performance of the BP-ANN model was the best compared with the other methods. The presented results illustrate that hyperspectral imaging technology is a powerful tool for prediction of moisture content of corn leaves.

ACKNOWLEDGEMENTS

Financial support from the Program for New Century Excellent Talents in University (NCET-12-0473), the National Science and Technology Supporting Plan (2011BAD29B08), the Sino-U.S. International Collaboration Project from MOST (2014DFG72150), and the National Natural Science Foundation of China (under Grant No. 61003151) is acknowledged. Data processing work by Pei Cao is acknowledged.

REFERENCES

Araújo, M. C. U., Saldanha, T. C. B., Galvão, R. K. H., Yoneyama, T., Chame, H. C., & Visani, V. (2001) The successive projections algorithm for variable selection in spectroscopic multicomponent analysis. *Chemomet. Intel. Lab. Syst., 57*(2),

65-73. http://dx.doi.org/ 10.1016/S0169-7439(01)00119-8.
Baiano, A., Terracone, C., Peri, G., & Romaniello, R. (2012). Application of hyperspectral imaging for prediction of physico-chemical and sensory characteristics of table grapes. *Comp. Elec. Agric., 87*, 142-151. http://dx.doi.org/10.1016/j.compag.2012.06.002.
Carter, G. A. (1991). Primary and secondary effects of water concentration on the spectral reflectance of leaves. *American J. Botany, 78*(7), 916-924. http://dx.doi.org/10.2307/2445170.
Cheng, X., Chen, Y. R., Tao, Y., Wang, C. Y., Kim, M. S., & Lefcourt, A. M. (2004). A novel integrated PCA and FLD method on hyperspectral image feature extraction for cucumber chilling damage inspection. *Trans. ASAE, 47*(4), 1313-1320. http://dx.doi.org/10.13031/2013.16565.
Danson, F. M., Steven, M. D., Malthus, T. J., & Clark, J. A. (1992). High-spectral resolution data for determining leaf water content. *Intl. J. Remote Sensing, 13*(3), 461-470. http://dx.doi.org/10.1080/01431169208904049.
Galvão, R. K. H., Araújo, M. C. U., Silva, E. C., José, G. E., Soares, S. F. C., & Paiva, H. M. (2007). Cross-validation for the selection of spectral variables using the successive projections algorithm. *J. Brazilian Chem. Soc., 18*(8), 1580-1584. http://dx.doi.org/10.1590/S0103-50532007000800021.
Gamal, E., & Jens, P. (2008). High-speed assessment of fat and water content distribution in fish fillets using online imaging spectroscopy. *Agric. Food Chem., 56*(17), 7672-7677. http://dx.doi.org/10.1021/jf801074s.
Geladi, P., Burger, J., & Lestander, T. (2004). Hyperspectral imaging: Calibration problems and solutions. *Chemomet. Intel. Lab. Syst., 72*(2), 209-217. http://dx.doi.org/10.1016/j.chemolab.2004.01.023.
Gowen, A. A., O'Donnell, C. P., Cullen, P. J., Downey, G., & Frias, J. M. (2007). Hyperspectral imaging: An emerging process analytical tool for food quality and safety control. *Trends Sci. Tech., 18*(12), 590-598. http://dx.doi.org/10.1016/j.tifs.2007.06.001.
Hatfield, J. L., & Pinter Jr., P. J. (1993). Remote sensing for crop protection. *Crop Prot., 12*(6), 403-414. http://dx.doi.org/10.1016/0261-2194(93)90001-Y.
Hernández-Hierro, J. M., Nogales-Bueno, J., Rodríguez-Pulido, F. J., & Heredia, F. J. (2013). Feasibility study on the use of near-infrared hyperspectral imaging for the screening of anthocyanins in intact grapes during ripening. *J. Agric. Food Chem., 61*(41), 9804-9809. http://dx.doi.org/10.1021/jf4021637.
Jackson, R. D. (1984). Remote sensing of vegetation characteristics for farm management. *Proc. SPIE 475: Remote Sensing: Critical Rev. Tech.*, 81-96. http://dx.doi.org/10.1117/12.966243.
Karimi, Y., Maftoonazad, N., Ramaswamy, H. S., Prasher, S. O., & Marcotte, M. (2012). Application of hyperspectral technique for color classification avocados subjected to different treatments. *Food Bioproc. Tech., 5*(1), 252-264. http://dx.doi.org/10.1007/s11947-009-0292-x.
Keshava, N. (2003). A survey of spectral unmixing algorithms. *Lincoln Lab. J., 14*(1), 55-73.
Kim, M. S., Chao, K., Chan, D. E., Jun, W., Lefcourt, A. M., Delwiche, S. R., Kang, S., & Lee, K. (2011). Line-scan hyperspectral imaging platform for agro-food safety and quality evaluation: System enhancement and characterization. *Trans. ASABE, 54*(2), 703-711. http://dx.doi.org/10.13031/2013.36473.
Li, J. B., Sun, Y. N., & Rao, X. Q. (2010). Detection of water content in corn based on hyperspectral imaging and neural network. *Packaging Food Mach., 28*(6), 1-4.
Liang, L., Yang, M. H., Zhang, L. P., Lin, H., & Zhou, X. D. (2012). Chlorophyll content inversion with hyperspectral technology for wheat canopy based on support vector regression algorithm. *Trans. Chinese Soc. Agric. Eng., 28*(20), 162-171.
Liu, L., & Ngadi, M. O. (2013). Detecting fertility and early embryo development of chicken eggs using near-infrared hyperspectral imaging. *Food Bioproc. Tech., 6*(9), 2503-2513. http://dx.doi.org/10.1007/s11947-012-0933-3.
Lorente, D., Blasco, J., Serrano, A. J., Soria-Olivas, E., Aleixos, N., & Gómez-Sanchis, J. (2013). Comparison of ROC feature selection method for the detection of decay in citrus fruit using hyperspectral images. *Food Bioproc. Tech., 6*(12), 3613-3619. http://dx.doi.org/10.1007/s11947-012-0951-1.
Nicolai, B. M., Beullens, K., Bobelyn, E., Peirs, A., Saeys, W., Theron, K., & Lammertyn, J. (2007). Nondestructive measurement of fruit and vegetable quality by means of NIR spectroscopy: A review. *Postharvest Biol. Tech., 46*(2), 99-118. http://dx.doi.org/10.1016/j.postharvbio.2007.06.024.
Noh, H. K., & Lu, R. (2007). Hyperspectral laser-induced fluorescence imaging for assessing apple fruit quality. *Postharvest Biol. Tech., 43*(2), 193-201. http://dx.doi.org/10.1016/j.postharvbio.2006.09.006.
Peñuelas, J., Filella, I., Biel, C., Serrano, L., & Save, R. (1993). The reflectance at the 950-970 nm region as an indicator of plant water status. *Intl. J. Remote Sensing, 14*(10), 1887-1905. http://dx.doi.org/10.1080/01431169308954010.
Peñuelas, J., Filella, I., Serrano, L., & Save, R. (1996). Cell wall elasticity and water index (R970nm/R900nm) in wheat under different nitrogen availabilities. *Intl. J. Remote Sensing, 17*(2), 373-382. http://dx.doi.org/10.1080/01431169608949012.
Qiao, J., Wang, N., & Ngadi, M. O. (2007). Pork quality classification using a hyperspectral imaging system and neutral network. *Intl. J. Food Eng., 3*(1), 1-12.
Talens, P., Mora, L., Morsy, N., Barbin, D. F., ElMasry, G., & Sun, D.-W. (2013). Prediction of water and protein contents and quality classification of Spanish cooked ham using NIR hyperspectral imaging. *J. Food Eng., 117*(3), 272-280. http://dx.doi.org/10.1016/j.jfoodeng.2013.03.014.
Tian, Y. C., Cao, W. X., Jiang, D., Zhu, Y., & Xue, L. H. (2005). Relationship between canopy reflectance and plant water content in rice under different soil water and nitrogen conditions. *Chinese J. Plant Ecol., 29*(2), 318-323.
Wang, H. W., & Meng, J. (2007). Predictive modeling on multivariate linear regression. *J. Beijing Univ. Aeronautics Astronautics, 33*(4), 500-504.
Wang, L., & Bai, Y. L. (2005). Correlation between corn leaf spectral reflectance and leaf total nitrogen and chlorophyll content under different nitrogen level. *Sci. Agric. Sinica, 38*(11), 2268-2276.
Xie, C. Q., Li, X. L., Nie, P. C., & He, Y. (2013). Application of time series hyperspectral imaging (TS-HSI) for determining water content within tea leaves during drying. *Trans. ASABE, 56*(6), 1431-1440.
Zhang, X. D., Mao, H. P., Zhou, Y., Zuo, Z. H., & Gao, H. Y. (2011). Study on detection of moisture content in lettuce leaves based on hyperspectral imaging technology. *J. Anhui Agric. Sci., 39*(33), 20329-20331.